

ISSN: (Print) (Online) Journal homepage: <https://www.tandfonline.com/loi/gcoo20>

The DNA- and protein-binding properties and cytotoxicity of a new copper(II) hydrazone Schiff base complex

Niladri Biswas, Sandeeptha Saha, Barun Kumar Biswas, Manas Chowdhury, Ashikur Rahaman, Vivek Junghare, Swati Mohapatra, Saugata Hazra, Ennio Zangrando, Ruma Roy Choudhury & Chirantan Roy Choudhury

To cite this article: Niladri Biswas, Sandeeptha Saha, Barun Kumar Biswas, Manas Chowdhury, Ashikur Rahaman, Vivek Junghare, Swati Mohapatra, Saugata Hazra, Ennio Zangrando, Ruma Roy Choudhury & Chirantan Roy Choudhury (2021) The DNA- and protein-binding properties and cytotoxicity of a new copper(II) hydrazone Schiff base complex, Journal of Coordination Chemistry, 74:9-10, 1482-1504, DOI: [10.1080/00958972.2021.1913128](https://doi.org/10.1080/00958972.2021.1913128)

To link to this article: <https://doi.org/10.1080/00958972.2021.1913128>



View supplementary material [↗](#)



Published online: 18 May 2021.



Submit your article to this journal [↗](#)



Article views: 55






View related articles [↗](#)



View Crossmark data [↗](#)



The DNA- and protein-binding properties and cytotoxicity of a new copper(II) hydrazone Schiff base complex

Niladri Biswas^a, Sandeeptha Saha^{a,b} , Barun Kumar Biswas^a, Manas Chowdhury^a, Ashikur Rahaman^c, Vivek Junghare^d, Swati Mohapatra^{d,f}, Saugata Hazra^{d,e} , Ennio Zangrando^g, Ruma Roy Choudhury^h and Chirantan Roy Choudhury^a 

^aDepartment of Chemistry, West Bengal State University, Kolkata, West Bengal, India; ^bSripur High School, Kolkata, West Bengal, India; ^cDepartment of Zoology, West Bengal State University, Kolkata, West Bengal, India; ^dDepartment of Biotechnology, Indian Institute of Technology Roorkee (IIT-R), Roorkee, Uttarakhand, India; ^eCentre for Nanotechnology, Indian Institute of Technology Roorkee (IIT-R), Roorkee, Uttarakhand, India; ^fAmity Institute of Microbial Technology, AU, Greater Noida, Uttar Pradesh, India; ^gDepartment of Chemical and Pharmaceutical Sciences, University of Trieste, Trieste, Italy; ^hDepartment of Chemistry and Environment, Heritage Institute of Technology, Kolkata, West Bengal, India

ABSTRACT

A new monomeric copper(II) benzhydrazone complex, [Cu(L)(H₂O)(NO₃)] (**1**), has been synthesized using Schiff base derived from quinoline-2-carboxaldehyde and benzhydrazide. Complex **1** was characterized by elemental analysis, FT-IR, UV-Vis spectroscopy along with electrochemical study and single-crystal X-ray crystallography. Single-crystal diffraction study of **1** indicates that the copper(II) ion adopts a distorted square pyramidal (SQP) geometry. The calf-thymus (CT) DNA-binding property of **1** has been evaluated by employing UV-vis and fluorescence spectroscopy, cyclic voltammetry and viscosity studies. The protein-binding ability of **1** was investigated by UV-vis and fluorescence spectroscopy titration using BSA and HSA. The significant interaction of **1** with CT-DNA was further supported by molecular docking approach. Finally, *in vitro* cytotoxicity of **1** was investigated by MTT assay on the Human Skin Carcinoma cell line A431. All these facts indicate that **1** exhibits a promising anticancer activity.


ARTICLE HISTORY

Received 29 August 2019
Accepted 15 March 2021

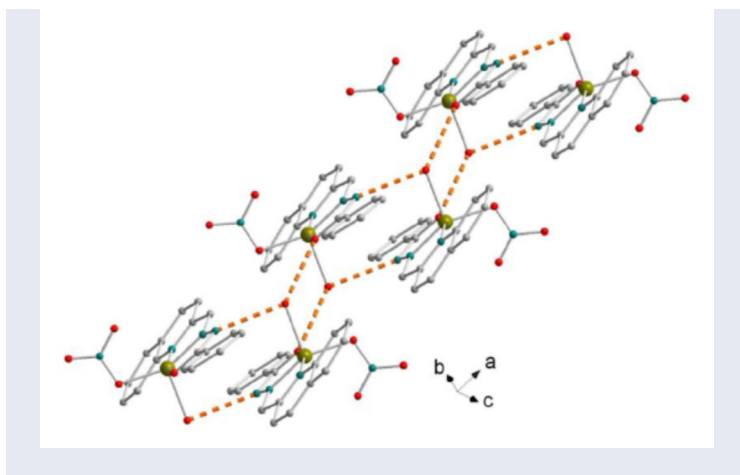
KEYWORDS

Copper(II); Schiff base complex; X-ray crystal structure; DNA-/protein-binding; molecular docking; Cytotoxicity

CONTACT Chirantan Roy Choudhury  crchoudhury2000@yahoo.com  Department of Chemistry, West Bengal State University, Kolkata, Kolkata, West Bengal, India

 Supplemental data for this article is available online at <https://doi.org/10.1080/00958972.2021.1913128>.

© 2021 Informa UK Limited, trading as Taylor & Francis Group



1. Introduction

Cisplatin is one of the most important chemotherapy drugs used to treat a number of cancers. However, platinum-based drugs have some limited use in medicinal applications because of their several side-effects, such as neurotoxicity, kidney problem, bone marrow suppression, allergic reactions as well as acquired drug resistance [1]. So, there were continued efforts over a few decades among bioinorganic chemists to develop an alternative to cisplatin, toward target-specific, less toxic and non-covalent DNA-binding drugs [2]. Extensive literature survey reveals that transition metal complexes of aryl hydrazones can act as effective inhibitors to cell growth as well as DNA-binding agents [3]. But the development of alternative metal-based drugs with zero side-effects still remains a challenge to the scientific community [1, 3].

First-row transition metals, especially iron, cobalt and copper, either alone or in their complexes, are essential in many living systems and involved in many biological processes [1]. Nanjundan *et al.* reported a series of first row transition metal complexes which were found to be most promising due to their large binding affinity toward calf-thymus DNA (CT-DNA) as well as toward bovine serum albumin (BSA), and the complexes were also active against the cervical cancer cell [4]. In life science, interaction between DNA and other molecules is a fundamental issue that relates the replication, transcription, mutation of genes and origin of some diseases [2]. Therefore, DNA is one of the main molecular targets to design effective chemotherapeutic agents and better anticancer drugs [5].

To find a solution of poor water solubility of metal complexes as anticancer drugs, protein biomolecules, *e.g.* HSA and BSA, are preferably used as carrier of drugs under investigation. Human serum albumin (HSA) is not only the most abundant protein in blood plasma but also plays a significant role in pharmacological study of drug distribution [6]. Another major soluble protein, BSA, is structurally similar to HSA and was found to be promising drug carrier that not only increases the solubility of metal compounds, but also enhances their antitumor activity [6,7]. Recently, interactions of metal

complexes with serum albumins have received much attention due to the pharmacodynamics and structure–activity relationships of antitumor metallopharmaceuticals [8].

Schiff base ligands are well-known to be synthetically interesting being able to readily form stable complexes with most of the transition metals [9]. Hydrazones and their derivatives, as stated above, have attracted much attention for their chelating capability and structural flexibility that can provide rigidity to the skeletal framework of the prepared metal complexes [10]. Very recently, copper(II)-hydrazone complexes have been found to be excellent anticancer agents as they induce apoptosis due to their potent DNA-binding/cleaving ability [1, 11].

Several desirable characteristics of hydrazones *e.g.* ease of preparation, increased hydrolytic stability relative to imines, and tendency toward crystallinity make them important pharmacophore units in the design and development of new biologically important metal complexes [3, 8, 12]. Quinoline and its analogues are of current interest for being potential compounds for the synthesis of compounds having excellent medicinal property [13].

Keeping in view the importance of the above-mentioned heterocyclic compounds, we have undertaken the synthesis of **1**, where the Schiff base ligand comprises benz-hydrazide moiety with the aim to investigate its biological activities *in vitro* [14]. The novel synthesized Cu(II)-Schiff base complex, $[\text{Cu}(\text{L})(\text{H}_2\text{O})(\text{NO}_3)]$ (**1**), was synthesized and characterized by elemental analysis, IR, UV-vis spectroscopy and single-crystal X-ray diffraction studies. Complex **1** was further investigated for its DNA- and protein-binding ability and cytotoxicity profile analysis. The DNA-binding was also supplemented by theoretical molecular docking study.

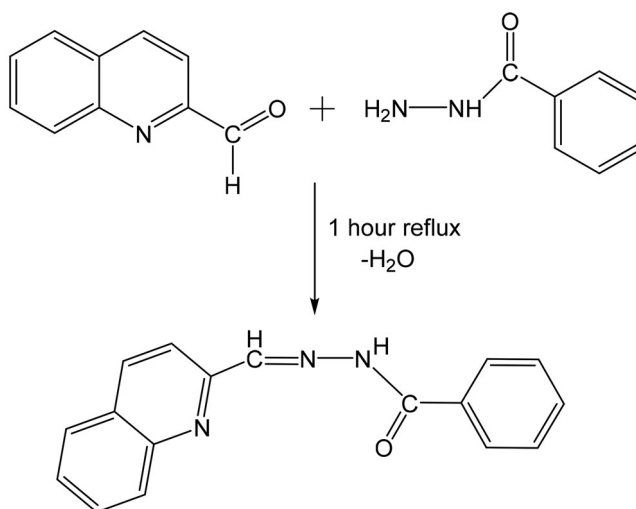
2. Experimental

2.1. Materials

Commercially available reagents and solvents were used without further purification during all synthetic work. Reagent grade $\text{Cu}(\text{NO}_3)_2 \cdot 3\text{H}_2\text{O}$ (E-Merck), quinoline-2-carboxaldehyde, benzohydrazide, TBAP and HSA (Sigma-Aldrich), BSA, CT-DNA and Tris-HCl buffer (SRL) and ethidium bromide (Spectrochem) were purchased from respective agencies as indicated in parenthesis. Tris-HCl buffer was prepared using deionized double distilled water and used for CT-DNA binding analysis.

2.2. Physical measurements

Elemental analysis of **1** was carried out on a Perkin-Elmer 2400 II elemental analyzer. Fourier Transform Infrared (FT-IR) spectra of HL and **1** were recorded from 400–4000 cm^{-1} on a Perkin-Elmer SPECTRUM – 2 FT-IR spectrophotometer as a solid KBr disc. Electronic spectra were recorded on a Perkin-Elmer Lambda-35 spectrophotometer of **1** with a concentration of 1.0×10^{-6} M using DMSO at 300 K. Emission data were recorded using DMSO on a Perkin-Elmer LS 55 fluorescence spectrophotometer at room temperature. Cyclic voltammetry of **1** was measured on a CH 660E electrochemical analyzer using a three electrode system with saturated calomel electrode (SCE) as reference, Pt wire-electrode as counter electrode and glassy carbon electrode



Scheme 1. Formation of Schiff base (HL).

as a working electrode at a scan rate of 50 mV sec^{-1} in dry nitrogen atmosphere. Electrochemical experiments were carried out in DMSO using 0.1 M TBAP as supporting electrolyte at 300 K. Electrospray mass spectra of HL and **1** have been recorded on a WATERS Xevo G2-S Q ToF mass spectrometer using HRMS grade acetonitrile and methanol as solvent, respectively. ^1H NMR spectrum of HL was recorded in DMSO-d_6 with a Bruker 400 MHz instrument using TMS as an internal standard.

2.3. Synthesis of Schiff base ligand (HL)

Hydrazone ligand was synthesized by refluxing equimolar solutions of quinoline-2-carboxaldehyde (0.786 g, 5 mmol) and benzhydrazide (0.681 g, 5 mmol) in 40 mL methanol for 1 h (Scheme 1). After that, a pale brownish product was formed and it was separated out from the solution. Then the product was filtered off and was washed with methanol and dried for characterization. Color: Pale brownish. Yield 78%. Anal. Calcd (%) for $[\text{C}_{17}\text{H}_{13}\text{N}_3\text{O}]$: C, 67.85; H, 5.35; N, 14.22. Found: C, 67.53; H, 4.97; N, 13.92. ^1H NMR (DMSO-d_6 , 400 MHz, 25°C), δ (ppm): 7.93 (1H, t), 8.28 (1H, d), 8.08 (1H, d), 8.39 (1H, s), 8.18 (1H, d), 7.89 (1H, d), 7.83 (1H, d), 7.76 (1H, d), 7.71 (1H, t), 7.61 (1H, t). FT-IR (KBr pellet), ν (cm^{-1}): 3196 (NH), 3063 (aromatic CH), 1675 (CO), 1562 (amide II), 1580 (C=N), 1493 (C=C). Electronic spectrum in DMSO solution, λ_{max} (nm): 235 ($\pi \rightarrow \pi^*$), 275 and 307 ($n \rightarrow \pi^*$). ESI-MS: (m/z) [found (calcd)]: 276.12 (275). The base peak was detected at $m/z = 276.12$, corresponding to $[\text{HL} + 1]^+$. FT-IR, UV-vis, NMR and mass spectra of HL are given in [Supplementary Information](#).

2.4. Synthesis of copper complex $[\text{Cu}(\text{L})(\text{H}_2\text{O})(\text{NO}_3)]$ (**1**)

Complex **1** was prepared by refluxing a methanolic solution of $\text{Cu}(\text{NO}_3)_2 \cdot 3\text{H}_2\text{O}$ (0.2416 g, 1 mmol) and hydrazone Schiff base ligand in 1:1 molar ratio for 2 h and the solution turned green. Then, the reaction mixture was filtered and left for

crystallization. After a few days, green single-crystals suitable for X-ray diffraction were obtained on slow evaporation and used for characterization. Yield: 68% (0.256 g). Anal. Calcd (%) for $[C_{17}H_{14}CuN_4O_5]$: C, 48.82; H, 3.35; N, 13.40. Found: C, 48.79; H, 3.33; N, 13.38. FT-IR (KBr pellet), ν (cm^{-1}): 3437(w), 1591(m), 1557(m), 1384(s), 1372(s), 1295(s), 513(s) and 474(s). Electronic spectrum in Tris-HCl buffer, pH 7.2, λ_{max} (nm): 277 ($\pi \rightarrow \pi^*$), 411 ($n \rightarrow \pi^*$) and 650 (d \rightarrow d). ESI-MS: (m/z) [found (calcd)]: 399.07 (399.87). [Given in [Supplementary Information](#)].

2.5. Single-crystal X-ray diffraction study

Diffraction data of **1** was collected at the X-ray diffraction beamline (XRD1) of the Elettra Synchrotron of Trieste (Italy) with a Pilatus2M image plate detector. Complete dataset was collected at 100 K with a monochromatic wavelength of 0.700 Å with the rotating crystal method. The crystal was dipped in N-paratone and mounted on the goniometer head with a nylon loop. The diffraction data were indexed, integrated and scaled using XDS [15]. The structure was solved by direct methods and subsequent Fourier analysis [16]. Refinement was performed by the full-matrix least-squares method based on F^2 implemented in SHELXL-2014 [16]. Anisotropic thermal motion was allowed for all non-hydrogen atoms. H atoms were included at calculated positions. All calculations were done with Wingx Version 2013.3 [17]; the molecular graphics were prepared using Cameron [18] and Diamond Ver 3.2k [19] programs.

2.6. DNA interaction experiments

2.6.1. Electronic absorption spectroscopy

Experiments involving the binding pattern of **1** with CT-DNA were studied in Tris-HCl buffer at pH 7.2 containing 1% DMSO as described previously [20]. The CT-DNA solution was prepared in Tris-HCl buffer medium and stored at 4 °C for complete dissolution and used within 4 days, and the concentration of CT-DNA was determined from its known molar extinction coefficient at 260 nm ($6600 \text{ M}^{-1} \text{ cm}^{-1}$). The UV absorbance A_{260}/A_{2680} signifies that CT-DNA was reasonably free from protein impurity [20]. In this particular experiment, the absorption titration spectra of **1** in the absence and presence of CT-DNA were recorded at fixed concentration of **1** ($50 \mu\text{M}$) but at different [complex **1**]/[CT-DNA] ratios. During measurements of the absorption spectra, equal incremental amounts of CT-DNA were added to both metal complex solution and reference solutions so that absorbance of CT-DNA can be detracted. During each titration, samples were equilibrated and prominent changes in absorption values were observed.

2.6.2. Competitive binding experiments

Competitive binding experiments were carried out as described in the literature [20]. Further support for the binding of **1** to CT-DNA was achieved by emission spectrometric techniques *via* ethidium bromide (EB) displacement assay. Due to quenching effect of solvent used, EB is normally non-emissive in Tris-HCl buffer at pH 7.2 containing 1% DMSO. Ethidium bromide enhanced its fluorescence intensity by interaction with CT-

DNA [21]. EB-displacement experiments were carried out by addition of the solution of **1** (0–60 μM) into a cuvette containing Tris-HCl buffer at pH 7.2 containing 1% DMSO solution of DNA-EB mixture ($[\text{DNA}] = 20 \mu\text{M}$, $[\text{EB}] = 10 \mu\text{M}$). The aliquot sample was excited at 510 nm and corresponding emission spectra were recorded from 520 to 750 nm. Fluorescence intensity at 610 nm was found to decrease after gradual addition of **1**.

2.6.3. Electrochemical studies

In order to determine the redox behavior of **1**, electrochemical investigation of **1** with CT-DNA was also carried out to determine the binding ability of the metal complex **1** with CT-DNA.

2.6.4. Viscosity measurements

A semi-micro viscometer was used for viscosity measurement of **1** at a constant temperature of 27 °C using a thermostatic water bath. Complex **1** (0–60 μM) was mixed with the CT-DNA solution (100 μM) and the change of viscosity was determined in each case. The flow time was measured with a digital stopwatch; each sample was measured at least three times and an average flow time was calculated. Relative viscosities for CT-DNA in the presence and absence of **1** were calculated; data were represented as $(\eta/\eta_0)^{1/3}$ versus binding ratio, where η is the viscosity of CT-DNA in the presence of **1** and η_0 is the viscosity of CT-DNA alone in Tris-HCl buffer at pH 7.2 containing 1% DMSO. Relative viscosity values were determined from the relation $\eta = (t-t_0)/t_0$, where t is the observed flow time of DNA containing **1** and t_0 is the flow time of Tris-HCl buffer itself [8, 22].

2.7. Protein-binding studies

The interactions between protein molecules (BSA and HSA) and **1** were studied using absorbance as well as fluorescence spectroscopic techniques. Fluorescence spectra were recorded from 300 to 500 nm with same excitation wavelength at 280 nm for both protein molecules. A stock solution of BSA and HSA protein (40 μM) was prepared in 50 mM Tris-HCl buffer medium with 1% DMSO at pH 7.2 [20] and stored in dark condition at 4 °C for further use. The fluorescence quenching experiments were performed by maintaining a fixed concentration of proteins and increasing concentrations of **1** (0–65 μM). The Stern-Volmer and Scatchard equations were employed to determine the type of interaction of **1** with protein molecules.

2.8. Molecular modeling and docking studies

The crystal structure of duplex DNA d(CGATCG)₂ hexamer (PDB ID: 1BNA) was retrieved from the Protein Data Bank (PDB). All water molecules and ligands were removed from the original PDB structure. Refinement and minimization of the extracted DNA was performed using receptor preparation wizard using OPLS3e force field. The refined structure of DNA was used for Receptor Grid generation. Complex **1** was modeled and minimized using LigPrep wizard, and being present a copper ion,

the added metal binding states option was chosen for generation of states for molecules. The Receptor grid was generated by 'Centroid for selected residues' option. All atoms of DNA were selected and grid generation job was run. The output file of grid generation i.e. '*maegz file*' was checked for successful preparation of grid. Then, the molecular docking was performed using Glide docking software of Schrodinger [23]. The extra precision (XP) docking was performed for generation of 10 poses. The *Perform post-docking minimization* was selected for minimization of the final docking complexes.

2.9. Cytotoxicity studies

2.9.1. Materials and methods for MTT assay

2.9.1.1. Cell lines and cultures. Human Skin Carcinoma cell line A431 was purchased from National Centre for Cell Science (NCCS), Pune, India, and was cultured in Dulbecco's Phosphate Eagle Medium (DMEM). The medium was supplemented with 10% Fetal Bovine Serum (FBS), 100 µg/mL streptomycin, and 100 IU/mL penicillin. The cell line was maintained in a humidified chamber having 5% CO₂ and 95% air at 37 °C.

2.9.1.2. Cell viability assay. The cytotoxic activity of **1** was determined by 3-(4,5-dimethyl-2-thiazolyl)-2,5-diphenyl-2H-tetrazolium bromide assay (MTT). The working stock solution of the compound was prepared by dissolving 10 mg of the compound in 1 mL of 50% dimethylsulfoxide (DMSO) making it a 10 mg/mL solution. Doxorubicin stock solution was also prepared by dissolving Doxorubicin Hydrochloride in DMSO. Cells were seeded in a 96 well plate with a cell density of 10,000 cells/well and were treated with various concentrations of the drug (from 10 mg/mL stock) for 24 h. For reference negative control (only media), vehicle control (with DMSO) and positive control (with doxorubicin 15 µg/mL) were used. The media after 24 h was discarded and the cells were rinsed with Phosphate Buffer Saline (PBS), pH = 7.4. 100 µL of fresh PBS was added to each well along with 10 µL of MTT solution (5 mg/mL) for 3 h and the formazon crystals were dissolved in DMSO and the absorbance was taken at 595 nm in a microplate reader.

The percentage of cytotoxicity was calculated as:

$$\% \text{ cell cytotoxicity} = (\text{OD control} - \text{OD treated}) / (\text{OD control}) \times 100$$

Data were represented in a bar plot as % of viability in x-axis vs. drug concentration in µg/mL in y-axis. The IC₅₀ dose was calculated using this plot and the data were represented as mean ± sd.

3. Results and discussion

3.1. Infrared spectral study

The FT-IR spectrum of **1** on a solid KBr disc is shown in Figure S2B. The IR-spectrum of mononuclear hydrazone complex displayed a broad band at 1591 cm⁻¹ due to azomethane stretching frequency ν(C=N) present in the complex. Complex **1** exhibited a band at 3437 cm⁻¹, which is characteristic of the N-H functional group. The

characteristic absorption bands at 758, 714, 697 and 614 cm^{-1} observed in the spectrum of **1** are due to low energy pyridine ring in-plane and out-of-plane vibrations, which are a good indication of the coordination of the heterocyclic nitrogen to the metal center [21, 24]. The appearance of two bands at 1557 and 1372 cm^{-1} can be attributed due to $\nu(\text{C}=\text{N}-\text{N}=\text{C})$ and $\nu(\text{C}-\text{O})$ stretching vibrations, respectively [3]. The IR spectrum of **1** showed bands at 487 and 513 cm^{-1} due to formation of M-N and M-O bonds, respectively. The presence of a strong band at 1384 cm^{-1} for **1** is due to $\nu(\text{N}-\text{O})$ stretching frequency and at 1295 cm^{-1} is attributed to the imidolate oxygen coordinated to copper. Finally, it can be concluded that the mode of coordination of the benzhydrazone ligand to copper(II) ion is realized *via* the azomethane nitrogen and imidolate oxygen.

3.2. Electronic spectral study

Electronic absorption spectrum of **1** in DMSO is shown in Figure S3B. The electronic spectrum of **1** showed a shoulder-like absorption band at 277 nm which can be assigned to intraligand $\pi \rightarrow \pi^*$ transition in the coordinated imines of the ligand. The high intensity absorption band appeared at 411 nm that can be attributed to $n \rightarrow \pi^*$ transition. A very low intensity band was observed at 650 nm in the visible region which corresponds to $d \rightarrow d$ transition.

3.3. Cyclic voltammetric study

Electrochemical studies were performed for **1** in DMSO under nitrogen atmosphere in the potential range from -2.0 to $+2.0$ V. Cyclic voltammogram of **1** is shown in Figure S4. The cyclic voltammetric response of oxidative wave at 0.80 V (*versus* SCE) is attributed to the oxidation of Cu(II) to Cu(III) and reductive wave at -0.90 V (*versus* SCE) is believed to be due to the reduction of Cu(II) to Cu(I) [21, 24].

3.4. X-Ray crystal structure

The crystallographically independent monomeric unit of **1** along with atom numbering scheme is shown in Figure 1. Crystal data and details of the structure determination for **1** are shown in Table 1. Selected bond lengths and angles are given in Table 2. The complex crystallizes as a five-coordinate monomeric species. The X-ray diffraction study indicates that the copper(II) ion adopts a distorted square pyramidal (SQP) geometry with $\tau = 0.118$, [$\tau = (\beta - \alpha)/60$, where β and α are the two largest angles around the central atom; $\tau = 0$ and 1 for the perfect square pyramidal and trigonal bipyramidal geometries, respectively] [25]. In the SQP geometry, the atoms forming the base are the quinoline (N1), the azomethine (N2) nitrogen atom and the oxygen atom (O1) from the tridentate Schiff base along with the oxygen atom (O2) from the nitrate anion. The aqua ligand O1W at the apical site completes the coordination geometry with a comparatively weaker Cu-O bond, which is typical of similar five-coordinate complexes and is consistent with the expected Jahn–Teller deformation along the apical axis [26].

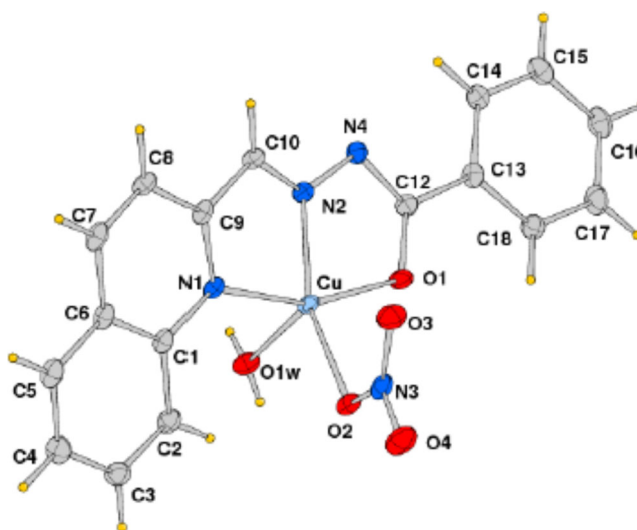


Figure 1. ORTEP view of **1** with displacement ellipsoids drawn at 50% probability level (hydrogens are omitted for clarity).

Table 1. Crystal data and details of the structure determination for **1**.

Empirical formula	$C_{17}H_{14}CuN_4O_5$
fw	417.86
Crystal system	Triclinic
Space group	$P - 1$
a, Å	7.6330(15)
b, Å	8.7770(18)
c, Å	12.587(3)
α , deg	80.56(3)
β , deg	82.12(3)
γ , deg	89.93(3)
V, Å ³	823.8(3)
Z	2
D _{calcd} , g cm ⁻³	1.685
μ (Mo-K α), mm ⁻¹	1.366
F(000)	426
θ range, deg	1.63 – 27.42
No. of reflns. collected	6422
No. of independent reflns.	3792
R _{int}	0.0502
No. of reflns. ($I > 2\sigma(I)$)	
No. of refined parameters	251
Goodness-of-fit (F^2)	1.228
R1, wR2 ($I > 2\sigma(I)$) ^(a)	0.0435, 0.1120
Residuals, e/Å ³	0.739, -1.491

The Schiff base is coordinated to the copper(II) ion in its iminoenolate form and the negative charge, generated upon deprotonation of the N4-H group, is delocalized across the O1–C12–N4 moiety, as indicated by the intermediate C12–N4 {= 1.338(2) Å} and C12–O1 bond distances {= 1.285(2) Å}. These bond lengths are to be compared with the value observed for C10–N2 {= 1.291(2) Å} and C=O bonds of carbonyl group (~1.2 Å). The nitrate ion is coordinated to the copper(II) ion *via* one of

Table 2. Selected bond lengths (Å) and angles (°) for **1**.

Bond	Bond length (Å)	Bond	Bond length (Å)
Cu-N(1)	2.0507(17)	Cu-O(2)	1.9895(15)
Cu-N(2)	1.9168(17)	Cu-O(1w)	2.2008(17)
Cu-O(1)	1.9849(14)		
Bond	Bond angle (°)	Bond	Bond angle (°)
N(2)-Cu-O(1)	78.83(7)	O(2)-Cu-N(1)	99.91(6)
N(2)-Cu-O(2)	152.67(6)	N(2)-Cu-O(1w)	114.36(7)
O(1)-Cu-O(2)	96.61(6)	O(1)-Cu-O(1w)	94.47(6)
N(2)-Cu-N(1)	81.09(7)	O(2)-Cu-O(1w)	92.77(6)
O(1)-Cu-N(1)	159.72(7)	N(1)-Cu-O(1w)	96.39(6)

the oxygen atoms. The torsion angles about the metal chelating units N2-N4-C12-O1 and N1-C9-C10-N2, upon complexation, are 1.5(2)° and −0.7(2)°, respectively, indicating almost planar conformation of atoms forming the five-membered rings around the metal center.

The monomers are connected through the H-bonds involving the water molecules connecting symmetry related complexes to form a zig-zag chain (Figure 2). In addition a few C-H...O interactions between quinoline ring and imino C-H with nitrato O2 and O3 oxygens are complementing to the conventional H-bonds to stabilize the packing of complexes in the lattice. Details of H-bonds are given in Table 3. Beside of this, there are a few C-H...O interactions between quinoline ring and imino C-H and the metal bound O2 as well as O3 of nitrato anion. The C-H...O interaction is complementing the conventional H-bond interactions between two adjacent monomeric units that stabilize the packing in the lattice.

3.5. DNA binding studies

3.5.1. Electronic absorption spectral studies

Before titration of **1** with CT-DNA, its stability in the Tris-HCl buffer solution containing 1% DMSO (pH ~7.2) [20] at room temperature was checked by UV-vis spectroscopy for 72 h but no distinguishable change was noticed (Figure S5A).

UV-Vis spectra of **1** in DMSO, Tris-HCl buffer medium containing 1% DMSO and acetonitrile were also compared (Figure S5B). No significant differences were noticed in the spectra taken in the three different solvents (Table S1 of Supplementary Information), indicating that **1** was stable under the experimental conditions. (For a detailed discussion on the integrity of **1** in aqueous medium, see Supplementary Information.)

Electronic absorption spectral technique is one of the important tools to determine the binding pattern of metal complexes with DNA which is determined by the change in absorption intensity of fixed concentration of metal complexes and also shifts in wavelength upon addition of DNA solution. Generally, of intercalative binding modes *e.g.* moderate, classical, *etc.*, of metal complexes is generally associated with hypochromism with or without red- or blue-shift [27]. The absorption titration spectra of **1** in the absence and presence of CT-DNA in Tris-HCl buffer medium is shown in Figure 3. After addition of increasing amounts of CT-DNA solution into **1**, the intensity

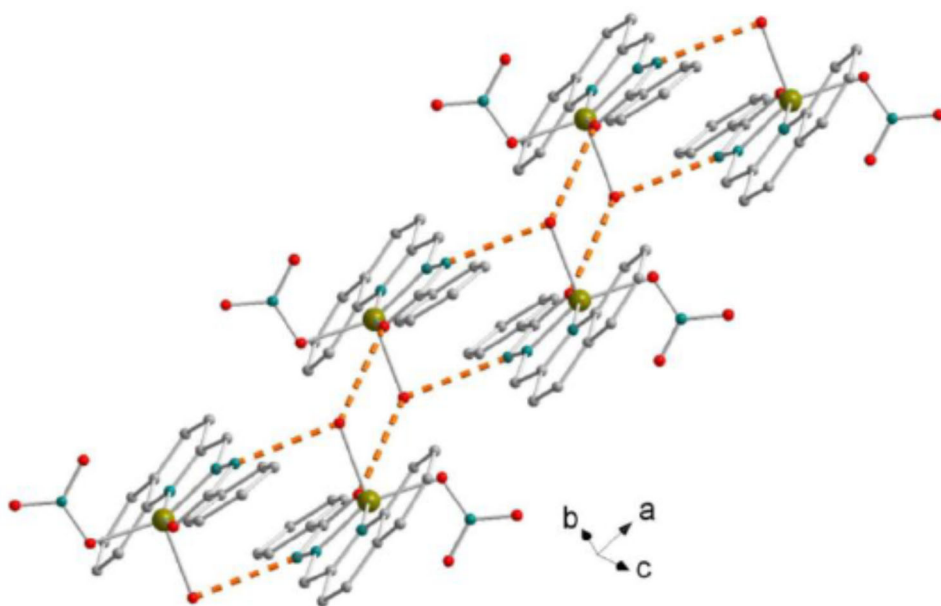


Figure 2. Packing diagram of **1** (dotted lines indicate H bonds involving water molecules Ow1).

Table 3. Hydrogen bonding parameters for **1**.

D – H...A	D – H [Å]	H...A [Å]	D...A [Å]	D – H...A [°]	Symmetry
O1w-H11...O1	0.83(3)	2.08(3)	2.908(2)	174(2)	-x, -y, 1-z
O1w-H12...N4	0.77(3)	2.18(3)	2.890(2)	154(3)	1-x, -y, 1-z
C2-H2...O2	0.9500	2.4700	3.160(2)	130.0	–
C5-H5...O3	0.9500	2.4000	3.291(3)	157.0	1-x, -y, -z
C10-H10...O2	0.9500	2.4000	3.186(2)	154.0	1+x, y, z

of $n-\pi^*$ transition band at 411 nm decreases and the intensity of $\pi-\pi^*$ transition band at 305 nm decreases along with prominent isosbestic point. 50% of hypochromism along with 4 nm hypsochromic shift was observed for the band at 411 nm upon incremental addition of CT-DNA. The observed hypochromic effect with blue-shift indicated that **1** interacts with CT-DNA [27]. During interaction of metal complex with the base pairs of DNA, the $\pi-\pi^*$ transition probability decreases and hence a hypochromism is generally observed [3].

In order to qualitatively determine the CT-DNA binding ability of **1** quantitatively, the intrinsic binding constant (K_b) was evaluated by the changes monitored in absorption intensity of $n-\pi^*$ transition band at 411 nm following the increasing CT-DNA concentration. The intrinsic binding constant (K_b) of **1** with CT-DNA was calculated with the following equation [21, 28]:

$$[\text{DNA}]/[\varepsilon_a - \varepsilon_f] = [\text{DNA}]/[\varepsilon_b - \varepsilon_f] + 1/K_b[\varepsilon_b - \varepsilon_f] \quad (1)$$

where [DNA] is the CT-DNA concentration in base pairs, the apparent extinction coefficient ε_a , ε_b and ε_f corresponds to $A_{\text{obs}}/[\text{compounds}]$, extinction coefficient of the complex when fully bound to CT-DNA and extinction coefficient of the complex in

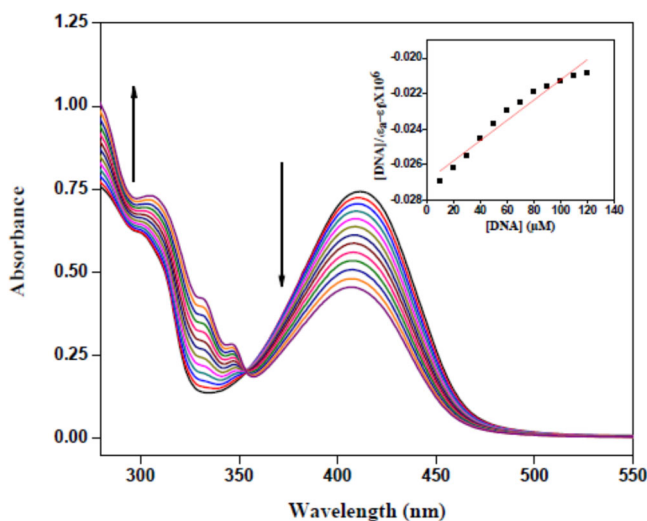


Figure 3. Electronic absorption spectra of **1** with CT-DNA in Tris-HCl buffer containing 1% DMSO. [Complex] = 50 μM , [CT-DNA] = 0–90 μM . The arrow shows the changes in the absorbance with the increasing amounts of CT-DNA. Inset shows the plot of $[\text{DNA}]/[\epsilon_a - \epsilon_f]$ versus $[\text{DNA}]$ for the measurement of intrinsic binding constant (K_b) of **1**.

unbound form. Plotting $[\text{DNA}]$ versus $[\text{DNA}]/[\epsilon_a - \epsilon_f]$ gave a slope $1/[\epsilon_a - \epsilon_f]$ and K_b was obtained from the ratio of the slope to y-intercept (Figure 3 inset). The value of K_b for **1** was found to be $6.465(\pm 0.052) \times 10^3 \text{ M}^{-1}$, and is lower than the typical classical intercalator EB, for which the binding constant was reported to be in the order of 10^6 M^{-1} [2]. The intrinsic binding constant (K_b) of previously reported related hydrazone-based metal complexes are in the range 10^3 – 10^5 M^{-1} [2, 8] while for other reported metal complexes also have same order of magnitude of K_b values [21, 29]. So, the electronic absorption study reveals that **1** behaves as partial intercalator or minor-groove binder with the base pairs of CT-DNA.

3.5.2. Competitive binding study by fluorescence spectroscopy

By using **1** as quencher, DNA binding ability of the complex was determined by decrease in the emission intensity of EB bound to DNA. Due to quenching effect of solvent used, EB is normally non-emissive in Tris-HCl buffer but, the emission is significant at around 610 nm when it binds to CT-DNA. When the quencher replaces EB, a decrease of the emission intensity of CT-DNA-EB mixture is observed [29]. Therefore, a competitive binding study was employed to investigate the mode of interaction of **1** with CT-DNA [21, 29]. The fluorescence quenching experiments were carried out by maintaining fixed concentration of CT-DNA (20 μM) in Tris-HCl buffer medium along with 10 μM EB and increasing aliquot amounts of aliquots of **1** (0–110 μM). Addition of **1** to the CT-DNA-EB system resulted in hypochromism of 78% accompanied by a bathochromic shift of 6 nm (Figure 4).

Complex **1** was able to displace some amount of EB from DNA-binding sites. The fluorescence quenching data was further analyzed by employing the Stern-Volmer relation [30]:

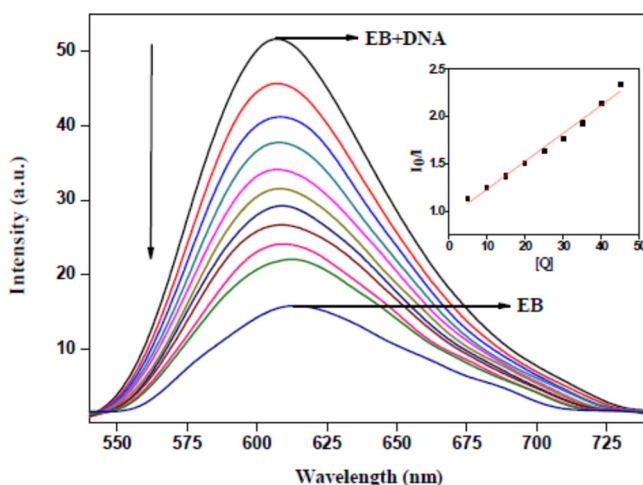


Figure 4. Fluorescence quenching curves of ethidium bromide bound CT-DNA in Tris-HCl buffer containing 1% DMSO by **1**. The arrow indicates the changes in the emission intensity on increasing copper complex concentration. [DNA] = 20 μ M, [EB] = 25 μ M and [Complex] = 0–45 μ M. The inset shows plot of I_0/I versus [Q].

Table 4. Stern-Volmer constant (K_{sv}), intrinsic binding constant (K_b), apparent binding constant (K_{app}), quenching rate constant (K_q) and number of binding sites (n) values of **1** in presence of CT-DNA.

K_{sv} (M^{-1})	K_b (M^{-1})	K_{app} (M^{-1})	K_q (M^{-1})	(n)
$3.533(\pm 0.014) \times 10^4$	$6.465(\pm 0.052) \times 10^3$	2.857×10^5	$3.533(\pm 0.014) \times 10^{12}$	1.11894 ± 0.03116

$$I/I_0 = 1 + K_{sv}[Q] = 1 + k_q\tau_0[Q] \quad (2)$$

where I_0 and I are the emission intensity in the absence and presence of the quencher molecule, respectively, K_{sv} is the linear Stern-Volmer quenching constant, $[Q]$ is the concentration of the quencher (complex **1**), k_q is the biomolecule quenching rate constant and τ_0 is the average life time of the fluorophore ($\sim 10^{-8}$ s) in the absence of the quencher. The linear Stern-Volmer quenching constant (K_{sv}) of **1** was obtained from the slope of the plot of I/I_0 vs. $[Q]$ and the calculated K_{sv} for **1** is $3.533(\pm 0.014) \times 10^4 M^{-1}$ (Table 4), indicating moderate binding affinity of **1** with CT-DNA. The observed K_q value of **1** is $3.533(\pm 0.014) \times 10^4 M^{-1}$, which is 100 times higher than the quenching rate constant value of $10^{10} M^{-1}s^{-1}$ [30].

The above observation indicates a static quenching mechanism where fluorophore and the quencher molecules possibly form ground state complex [27]. Further, the apparent CT-DNA binding constant (K_{app}) of **1** was determined using the following equation [8],

$$K_{EB}[EB] = K_{app}[\text{complex}] \quad (3)$$

where K_{EB} is $1.0 \times 10^6 M^{-1}$, the EB concentration is 10 μ M and [complex] is the concentration of **1** that causes a decrease of 50% in emission intensity of EB. The apparent binding constant (K_{app}) of **1** in the range of $10^5 M^{-1}$ (Table 4) indicates a moderate binding ability of **1** with CT-DNA [21, 29]. The K_{app} value of **1** is comparable with those of previously reported copper hydrazone complexes [14], but much lower

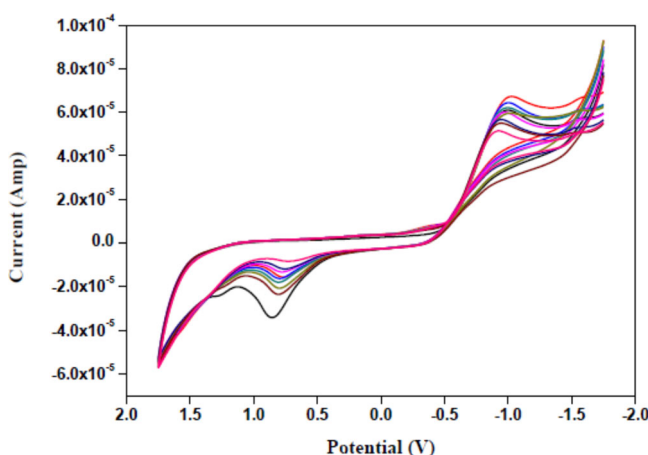


Figure 5. The cyclic voltammogram of **1** at various concentrations of CT-DNA in Tris-HCl buffer medium containing 1% DMSO at a scan rate of 50 mV sec⁻¹ in Tris-HCl buffer.

than that of typical classical intercalator EB [29,30]. In order to determine the number of binding sites (n), the Scatchard equation [21, 29] was employed:

$$\log [(I_0 - I)/I] = \log K_b + n \log [Q] \quad (4)$$

The slope of the plot of $\log [(I_0 - I)/I]$ vs. $\log [Q]$ (Figure S6) provides the number of binding sites to **1** in CT-DNA (Table 4). It can be concluded that **1** shows static quenching phenomenon and moderate binding affinity with CT-DNA and also a comparatively lower binding interaction with CT-DNA than that of EB with CT-DNA. So in this case, one reason may be that the fluorescence quenching of EB-DNA may happen due to the replacement of EB by **1**. It may also be caused by the EB-DNA-complex **1** conjugate and due to FRET, so the quenching of fluorescence may take place [31].

3.5.3. Electrochemical study

The cyclic voltammetry was used as complementary study to support and to reinforce result of spectral analysis [28]. The redox behavior of a metal complex in the presence of biologically important molecule is investigated in a very sensitive way by this technique [27, 32] (Figure 5).

The concentration of CT-DNA in Tris-HCl buffer medium (pH = 7.2) was varied while that of **1** was kept constant. Cyclic voltammogram of **1** shows an irreversible oxidation peak potential at 0.80 V (*versus* SCE) and irreversible reduction peak potential at -0.87 V (*versus* SCE). After incremental addition of CT-DNA to the solution of **1** containing 0.1 M TBAP, the oxidation peak at 0.80 V shifted to a more negative value of 0.75 V, and the reduction peak at -0.87 V also shifted significantly to a more positive value of -0.80 V. It was observed that heights of both the anodic and cathodic peak currents decreased in the same fashion during the addition of increasing amounts of CT-DNA, which suggests the binding of slowly diffusing DNA molecules to **1** [27, 32]. The shift of reduction peak potential toward a more positive value for the incremental addition of CT-DNA solution signifies electron deficiency

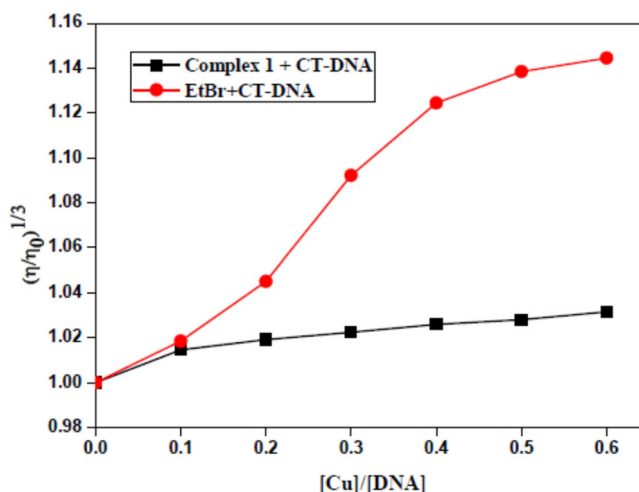


Figure 6. Effect of increasing concentration of **1** (10–60 μM) on relative specific viscosity of CT-DNA solution at fixed concentration (10 μM) at 27 $^{\circ}\text{C}$.

due to the interaction of **1** with the base pairs of CT-DNA double strands. The behavior was further supported by shift of oxidation peak potential to a more negative value, quite similar to the previously reported copper(II) hydrazone complex [14]. Therefore, the study of cyclic voltammogram of **1** in the absence and presence of CT-DNA (Figure 5) indicates a sort of interaction between the titled complex and the DNA base pairs through which the electron cloud from the complex is dragged toward the CT-DNA strands [14, 21].

3.5.4. Viscosity study

In order to investigate in detail the binding mode of CT-DNA with the metal complex, viscosity measurements were performed for CT-DNA in the absence and presence of **1**. This is a very sensitive technique to indicate the change in length of DNA-base pairs [33]. It has been shown that viscosity of CT-DNA increases when a metal complex strongly intercalates into the base pairs while no change in viscosity in the case of electrostatic interaction between metal complex and CT-DNA [22, 33]. However, any variation in viscosity implies a small change in the effective length of DNA double helix. This happens when a metal complex forms a curve in a DNA molecule called a non-classical or partial intercalative binding mode [29, 33]. The effect of the copper(II) benzhydrazone complex on the CT-DNA viscosity is shown in Figure 6.

Figure 6 shows that there was very small enhancement in the relative viscosity of CT-DNA upon incremental addition of **1**, in CT-DNA while a significant increase was observed when EB concentration in CT-DNA was gradually increased. The standard slope of viscosity curve of CT-DNA with the classical intercalator EB is 0.96 [21, 34], but much lower value of 0.27 is obtained in the case of **1** with CT-DNA. The smaller binding constant of **1** compared to that of EB implies a non-classical, partial intercalative binding or groove binding mode of **1** with CT-DNA, supporting the preliminary indications derived from absorption spectroscopy studies.

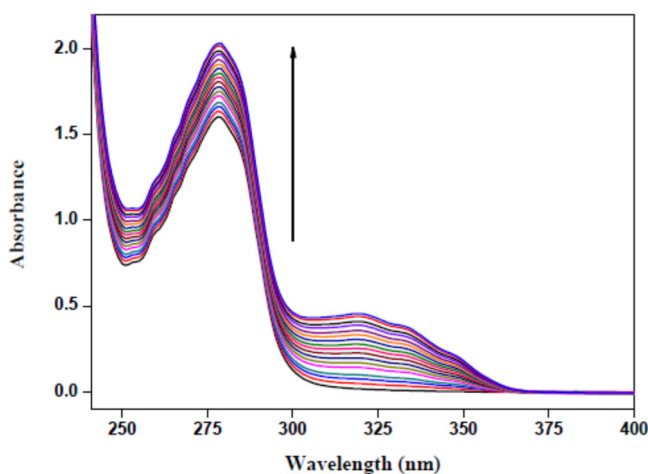


Figure 7. Absorption titration spectra of BSA [40 μM] with increasing concentration [0–85 μM] of **1** at room temperature in Tris-HCl buffer medium containing 1% DMSO.

3.6. Protein-binding studies

3.6.1. Uv-vis absorption measurements

UV-vis absorption spectral measurement was done to determine the structural change as well as the type of quenching of protein molecules (BSA and HSA) upon addition of the metal complex. Two types of quenching mechanisms, namely static or dynamic, are observed for protein molecules [35]. In case of static quenching, a considerable change in absorption spectra of fluorescent molecule occurs due to formation of new compound between the fluorescent molecule in ground state and the quencher [35]. But, no considerable change in absorption spectra is observed in the case of dynamic quenching because only excited state of the fluorescent compound is influenced by the quenchers. The absorption spectra of BSA and HSA with absorption maxima at 279 nm in the presence of **1** are shown in Figures 7 and S7, respectively.

Upon continuous addition of **1** to the solutions of BSA and HSA, the absorption maxima at 279 nm increased significantly with a gradual blue-shift. This indicates a ground state complex formation between the protein molecules and **1** which is observed in static quenching mechanism. An analogous static quenching phenomenon between proteins with metal complexes has been reported [1, 33].

3.6.2. Fluorescence spectral study

Qualitative analysis of interaction of **1** to the most abundant blood proteins, BSA and HSA, is generally investigated by examining their fluorescence spectra [22]. In general, tryptophan, tyrosine and phenylalanine are the three intrinsic residues responsible for intense fluorescence of a protein molecule [36]. Among these, phenylalanine has a very low quantum yield and ionization of tyrosine completely reduces the fluorescence of protein molecules. Therefore, the intrinsic fluorescence of protein molecule is mainly due to the presence of tryptophan and tyrosine moieties [36]. According to the fluorescence of protein molecules, both the serum albumins were excited at 278 nm and strong intense fluorescence were observed at 346 and 343 for BSA and HSA,

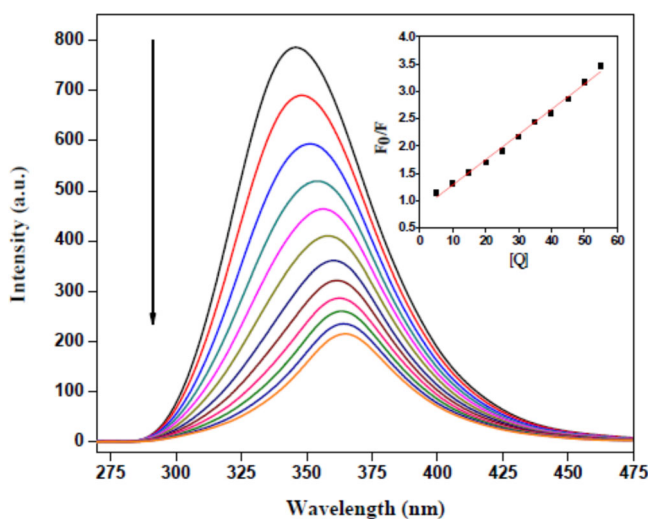


Figure 8. The fluorescence quenching curves of BSA (40 μM ; $\lambda_{\text{exc}} = 278 \text{ nm}$; $\lambda_{\text{emi,max}} = 346 \text{ nm}$) with increasing concentration of **1** (0–55 μM), indicated by the arrow. The inset shows the Stern-Volmer linear plot of F_0/F versus $[Q]$ of **1** with BSA.

respectively, due to tryptophan moiety [36]. Figures 8 and S8 show the gradual decrease of strong emission intensities of BSA and HSA solutions (40 μM) due to gradual addition of **1** (0–60 μM).

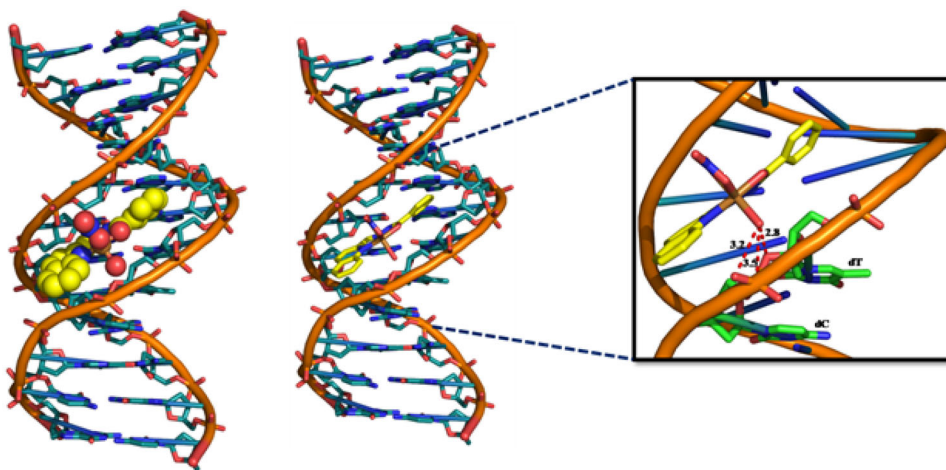
The intense emission band at 346 and 343 nm for BSA and HAS, respectively, gradually reduced along with significant red-shift due to the addition of **1**, indicating possible interaction of **1** with proteins. The observed quenching may be attributed to possible changes in the tryptophan environment of protein molecules leading to changes in the secondary structure of protein that ultimately indicates binding of **1** with BSA and HSA [35]. There may be a possible energy transfer from the indole unit of the tryptophan to the compound under study leading to the shifting of the emission maxima toward higher wavelengths [30]. The fluorescence quenching mechanism in the complex-protein system can be deduced using the classical Stern-Volmer equation [21, 26],

$$F_0/F = 1 + K_{\text{sv}}[Q] = 1 + K_{\text{q}}\tau_0 \quad (5)$$

where F_0 and F represent the fluorescence intensities of fluorophore in the absence and presence of a quencher, respectively, K_{sv} and K_{q} are linear Stern-Volmer quenching constant and the quenching rate constants of biomolecules, respectively, τ_0 is quenching rate constant of biomolecules (10^{-8} s) for tryptophan fluorescence in proteins [36] and $[Q]$ is the quencher concentration. The K_{sv} and K_{q} values for **1** are shown in Table 5. However, the maximum scatter collision quenching constant, K_{q} , for various quenchers with the biopolymers is $2 \times 10^{10} \text{ M}^{-1}\text{s}^{-1}$ [36]. Thus, the rate constant calculated by the protein quenching procedure is 100-fold higher than K_{q} of the scatter procedure. These results indicate that the specific interaction between copper(II) benzhydrazone complex and proteins and the probable quenching mechanism was not initiated by a dynamic quenching but rather by a static one [21, 26]. The

Table 5. Stern-Volmer constant (K_{sv}), quenching rate constant (K_q), binding constant (K_b), and number of binding sites (n) of Cu(II) benzhydrazone complex in presence of BSA and HSA.

Proteins	$K_{sv} (M^{-1})$	$K_q (M^{-1})$	$K_b (M^{-1})$	(n)
BSA	$4.607(\pm 0.001) \times 10^4$	$4.607(\pm 0.001) \times 10^{12}$	$4.442(\pm 0.074) \times 10^5$	1.23037 ± 0.01607
HSA	$5.593(\pm 0.003) \times 10^4$	$5.593(\pm 0.003) \times 10^{12}$	$4.881(\pm 0.183) \times 10^5$	1.23649 ± 0.03965

**Figure 9.** DNA-complex 1 interaction.

binding constants (K_b) and the number of binding sites (n) to **1** in protein molecules were obtained from the Scatchard equation [21, 26],

$$\log [(F_0 - F)/F] = \log K_b + n \log [Q] \quad (6)$$

The plots of $\log [(F_0 - F)/F]$ versus $\log [Q]$ (Figures S9A and S9B for BSA and HSA, respectively) and K_b and n values are listed in Table 5. These values indicate that **1** quenches more strongly with BSA than HSA in static quenching mode.

3.7. Molecular docking of **1** with DNA

The glide binding energy is the Glide scoring function which calculates the score by taking in consideration of receptor-ligand interactions by calculating Coulomb - van der Waals energies, hydrogen bond terms, lipophilic-lipophilic term and a rotatable bond penalty calculated and shown in Supplementary table S2. The distribution of the intermolecular energies have been decrypted in Supplementary table S3. The pose number is actually a ranking of this poses based on docking score *i.e.* glide score. The pose index, penalty represents the index for a pose in occurrence and protonation penalty for unlikely protonation states, respectively. The remaining are the different interaction energies between **1** and DNA.

The docking grid was generated by selecting all atoms of DNA. This docking was concluded in the binding of all poses in the minor groove. Thus, the lowest energy pose was found to be a suitable candidate to consider as a possible complex **1** binding pose with DNA. According to table S2, pose number 1 has been found to be the lowest energy conformation, which is -0.878 kcal/mol. The conformation of **1** has

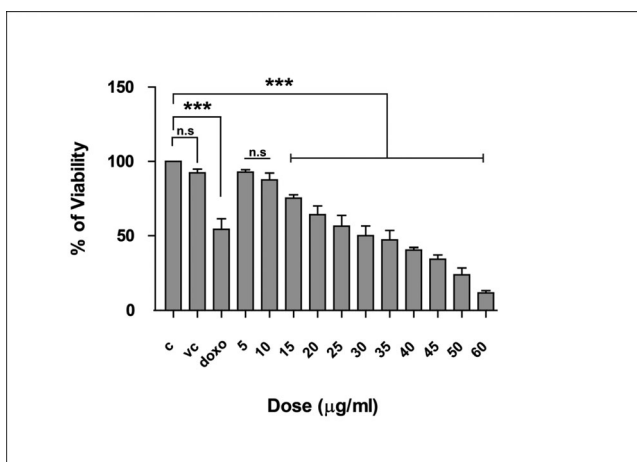


Figure 10. A431 cell viability measured by MTT assay at various concentrations of **1**.

been found to be planar around a copper atom where the rings were present (Figure S10). It made to fit it in the minor groove of DNA. The residue thionine (dT8) and cytosine (dC9) of DNA from chain A was found to be interacting with **1**. The electro-positive nature of copper from **1** induces a partial electronegative charge on the oxygen attached to it and that might have resulted in this binding. The thionine (dT8) has oxygen O3 which formed a polar contact with the oxygen of **1** at 2.8 Å. Similarly, the oxygen OP1 from cytosine (dC9) had a distance 3.2 Å from the oxygen of **1** and phosphorus, P, of dC9 was at distance ~3.5 Å from **1** (Figure 9). The intermolecular hydrogen bond energy of pose 1 is highest among all other poses, which is -0.7 kcal/mol. So this can be treated as a possible interaction that makes **1** show good binding with DNA. Thus, docking study poses that the probable binding of **1** is in the minor groove of a DNA and also provides the nature of its binding.

3.8. Cytotoxicity profile study

The cytotoxic activity of **1** was studied in the A431 skin cancer cell line *in vitro* using MTT assay. A well-known anticancer drug, Doxorubicin, was used as a reference standard. The cytotoxic activity shows that the vehicle (DMSO) used was unable to induce significant toxicity in skin cancer cells but the compound induces cytotoxicity in A431 cells in a dose-dependent manner with IC_{50} of $78.7 \pm 0.53 \mu M$. Cell viability study of A431 cell line by MTT assay at various concentrations of **1** is shown in Figure 10.

It is well-known that coordination of central metal ion with coordinating ligand and the stereochemistry of the resultant metal complex is the key for the cytotoxic potential of the resultant metal complex [37]. The cytotoxic activity of **1** is compared with other similar complexes found in literature and shown in Table 6 [38–47]. Here it is evident that cytotoxic potential of synthesized complex mainly depends on the coordination stereochemistry and nature of substituents present in the aromatic ring of the Schiff base. [37]. In this case, **1** possesses square pyramidal geometry and is non-

Table 6. Representative examples of metal complexes along with **1** for cytotoxicity study (IC_{50} , in μM) on A431 cell line.

Compound	A431 (IC_{50} , in μM)	References
1. $[Cu(L)(H_2O)(NO_3)]$	78.7 ± 0.53	Current work
2. Doxorubicin	27.6 ± 0.58	Current work
3. <i>cis</i> -platin	16.8 ± 0.07	[38]
4. $[RuCl_2(PPh_3)(L_1)]$	27.2 ± 0.17	[38]
5. $[RuCl_2(PPh_3)(L_2)]$	89.3 ± 0.1	[38]
6. $[RuCl_2(PPh_3)(L_3)]$	19.2 ± 0.09	[38]
7. $[RuCl_2(PPh_3)(L_4)]$	31.1 ± 0.2	[38]
8. $[Py_3Co(L_5)]$	11.3 ± 2.7	[39]
9. $[Py_3Co(L_6)]$	16.3 ± 1.8	[39]
10. $[Ni(L_7)_2]$	80.72	[3]
11. $[Ni(L_8)_2]$	35.13	[3]
12. $[Cu(L_9)(PPh_3)_2]$	132 ± 1	[40]
13. $[Cu(L_{10})(PPh_3)_2]$	97 ± 1	[40]
14. $[Cu(L_{11})]$	2.6	[41]
15. $[Co(L_{12})_2]$	32.12 ± 1.03	[42]
16. $[Co(L_{13})_2]$	16.85 ± 2.09	[42]
17. $[Co(L_{14})_2]$	9.30 ± 0.03	[42]
18. $[Co(L_{15})_2Cl]$	32.12 ± 1.03	[43]
19. $[Co(L_{16})_2Cl]$	16.85 ± 2.09	[43]
20. $[Co(L_{17})_2Cl]$	9.30 ± 0.03	[43]
21. $[(L_{18}H)Cu(PPh_3)_2](PF_6)$	0.6 ± 0.1	[44]
22. $[(L_{19}H)Cu(PPh_3)_2](PF_6)$	2.75 ± 0.5	[44]
23. $[(L^{1NMDA})Cu(PPh_3)_2](PF_6)$	0.2 ± 0.01	[44]
24. $[(L^{2NMDA})Cu(PPh_3)_2](PF_6)$	0.61 ± 0.1	[44]
25. $[(L_{18}H)Cu(PTA)_2](PF_6)$	2.8 ± 1.2	[44]
26. $[(L_{19}H)Cu(PTA)_2](PF_6)$	0.2 ± 0.003	[44]
27. $[(L_1NMDA)Cu(PTA)_2](PF_6)$	3.3 ± 0.7	[44]
28. $[(L_2NMDA)Cu(PTA)_2](PF_6)$	3.2 ± 0.3	[44]
29. $[Ru(CO)(PPh_3)(L_{20})]$	9.30	[45]
30. $[Ru(CO)(PPh_3)(L_{21})]$	26.70	[45]
31. $[Ru(CO)(PPh_3)(L_{22})]$	16.87	[45]
32. $[Ru(CO)(AsPh_3)(L_{23})]$	42.64	[45]
33. $[Cu(L_{24})Br_2]$	3.18	[46]
34. $[Pt(dipy)Cl_2]$	58.13 ± 0.71	[47]
35. $[Pt_2(\mu-OH)_2(dipy)_2](NO_3)_2 \cdot 2H_2O$	0.98 ± 1.10	[47]
36. $[Pt_2(\mu-S-aet)_2(dipy)_2](NO_3)_4 \cdot 2H_2O$	189.52 ± 1.21	[47]
37. <i>cis</i> - $[Pd(NH_3)_2Cl_2]$	25.42 ± 0.97	[47]
38. $[Pd(dipy)Cl_2]$	38.27 ± 1.25	[47]
39. $[Pd_2(\mu-OH)_2(dipy)_2](NO_3)_2 \cdot 2H_2O$	0.02 ± 0.85	[47]
40. $[Pd_2(\mu-S-aet)_2(dipy)_2](NO_3)_4$	132.91 ± 1.18	[47]

HL₁ = 1,2-naphthoquinone thiosemicarbazone (C₁₁H₉N₃OS), HL₂ = 1,2-naphthoquinone methylthiosemicarbazone (C₁₂H₁₁N₃OS), HL₃ = 1,2-naphthoquinone phenylthiosemicarbazone (C₁₇H₁₃N₃OS), HL₄ = 1,2-naphthoquinone semicarbazone (C₁₁H₉N₃O₂), L₅ = 3,5-ClC₆H₂(O)C = NC₆H₃(O)-4-NO₂, L₆ = 3,5-BrC₆H₂(O)C = NC₆H₃(O)-4-NO₂, HL₇ = [Cp₂Fe(CH = N-NH-CO-C₆H₅)], HL₈ = [Cp₂Fe(CH = N-NH-CO-C₅H₄N)], HL₉ = C₁₆H₁₄N₂O₂Fe₁, HL₁₀ = C₁₆H₁₄N₂O₁SiFe₁, L₁₁ = ethyl 2-(2-(2-chlorobenzoyl)hydrazono)propanoate (C₁₂H₁₃ClN₂O₃), L₁₂ = C₁₄H₁₈N₁₀S, L₁₃ = C₁₅H₂₀N₁₀S, L₁₄ = C₂₀H₂₂N₁₀S, HL₁₅ = 2-acetylpyridine-thiosemicarbazone (C₈H₁₀N₄S), HL₁₆ = 2-acetylpyridine-4-methyl-thiosemicarbazone (C₉H₁₂N₄S), HL₁₇ = 2-acetylpyridine-4-phenyl-thiosemicarbazone (C₁₄H₁₄N₄S), HL₁₈ = bis(pyrazol-1-yl) carboxylic acid, HL₁₉ = bis(3,5-dimethylpyrazol-1-yl) carboxylic acid, L^{1NMDA} or L^{2NMDA} = bis(pyrazol-1-yl) acetates conjugated with an N-methyl-D-aspartate (NMDA) receptor antagonist (L^{1NMDA} or L^{2NMDA}) and phosphane ligands (triphenylphosphine or 1,3,5-triaza-7-phosphaadamantane), L₂₀ = bis(salicylaldehyde)-S-methylisothiosemicarbazone (C₁₆H₁₃O₂N₃S), L₂₁ = bis(5-chlorosalicylaldehyde)-S-methylisothiosemicarbazone (C₁₆H₁₃O₂N₃Cl₂S), L₂₂ = bis(o-vanillin)-S-methylisothiosemicarbazone (C₁₈H₁₉O₄N₃S), L₂₃ = bis(2-hydroxynaphthaldehyde)-S-methylisothiosemicarbazone (C₂₄H₁₉O₂N₃S). L₂₄ = N,N'-(pyridine-2-ylmethylene)dehydroabietylamine (C₃₂H₄₁N₃).

planar. So, the activity of **1** is relatively less compared to the similar more planar complexes in the literature [38–47]. Nevertheless, **1** can be considered as a potential candidate in cancer therapy with IC_{50} value of $78.7 \pm 0.53 \mu M$. This complex is somewhat less effective compared to standard drugs, *cis*-platin or doxorubicin (Table 6).

4. Conclusion

- a. A new copper(II) complex (**1**), [Cu(L)(H₂O)(NO₃)], has been synthesized using a tridentate benzhydrazone Schiff base ligand with NNO donor set. Complex **1** was fully characterized by spectral, analytical along with single-crystal X-ray diffraction study.
- b. Through a variety of spectroscopic studies, **1** was shown to exhibit prominent propensity to interact with CT-DNA and BSA/HSA biomolecules.
- c. The DNA-binding property of **1** was examined using UV-vis, fluorescence, cyclic voltammetry and viscosity study. The moderate intercalative groove binding pattern of **1** with DNA was confirmed by its low intrinsic binding constant value and was also supported by molecular docking study.
- d. A significant static quenching phenomenon of **1** with BSA and HSA was investigated by UV-Vis as well as fluorescence study.
- e. The MTT assay clearly indicated that **1** represents an optimistic drug for the Human Skin Carcinoma cell line A431 with IC₅₀ value of $78.7 \pm 0.53 \mu\text{M}$.

Supplementary data

CCDC 1938884 contains the supplementary crystallographic data for **1**. These data can be obtained free of charge via <http://www.ccdc.cam.ac.uk/conts/retrieving.html>, or from the Cambridge Crystallographic Data Centre, 12 Union Road, Cambridge CB2 1EZ, UK; Fax: (+44) 1223-336-033; or E-mail: deposit@ccdc.cam.ac.uk. Supplementary data associated with this article can be found in the online version.

Acknowledgements

N. Biswas acknowledges CSIR, New Delhi, Govt. of India, for awarding junior research fellowship (Project No: 01/2537/11 - EMR - II). C. Roy Choudhury acknowledges DST-FIST (Project No. SR/FST/CSI-246/2012) New Delhi, Govt. of India for instrumental support under capital heads.

Disclosure statement

No potential conflict of interest was reported by the authors.

ORCID

Sandeeptha Saha  <http://orcid.org/0000-0002-7562-5932>

Saugata Hazra  <http://orcid.org/0000-0002-3074-1534>

Chirantan Roy Choudhury  <http://orcid.org/0000-0003-3095-3040>

References

- [1] B. Deka, T. Sarkar, S. Banerjee, A. Kumar, S. Mukherjee, S. Deka, K.K. Saikia, A. Hussain. *Dalton Trans.*, **46**, 396 (2017).
- [2] S.M. Pradeepa, H.S.B. Naik, B.V. Kumar, K.I. Priyadarsini, A. Barik, S. Jayakumar. *Inorg. Chim. Acta*, **428**, 138 (2015).

- [3] K. Sudeepa, N. Narsimsa, B. Aparna, S. Sreekanth, A.V. Aparna, M. Ravi, J. Mohmed, C.S. Devi. *J. Chem. Sci.*, **130**, 52 (2018).
- [4] D. Dey, S. Das, H.R. Yadav, A. Ranjani, L. Gyathri, S. Roy, P.S. Guin, D. Dhanasekaran, A.R. Choudhury, M.A. Akbarsha, B. Biswas. *Polyhedron*, **106**, 106 (2016).
- [5] S. Mondal, M. Chakraborty, A. Mondal, B. Pakhira, A.J. Blake, E. Sinn, S.K. Chattopadhyay. *New J. Chem.*, **42**, 9588 (2018).
- [6] Y. Gou, Y. Zhang, J. Qi, Z. Zhou, F. Yang, H. Lian. *J. Inorg. Biochem.*, **144**, 47 (2015).
- [7] Y.R. Zheng, K. Suntharalingam, T.C. Johnstone, H. Yoo, W. Lin, J.G. Brooks, S.J. Lippard. *J. Am. Chem. Soc.*, **136**, 8790 (2014).
- [8] R.R. Kumar, R. Ramesh. *RSC Adv.*, **5**, 101932 (2015).
- [9] M. Dehkhodaei, M. Sahihi, H.A. Rudbari, F. Momenbeik. *J. Biol. Inorg. Chem.*, **23**, 181 (2018).
- [10] H.G. Aslan, S. Ozcan, N. Karacan. *Inorg. Chem. Commun*, **14**, 1550 (2011).
- [11] J.A. Lessa, I.C. Mendes, P.R.O. da Silva, M.A. Soares, R.G. dos Santos, N.L. Speziali, N.C. Romeiro, E.J. Barreiro, H. Beraldo. *Eur. J. Med. Chem.*, **45**, 5671 (2010).
- [12] Y. Li, Z. Yang, M. Zhou, Y. Li. *RSC Adv.*, **7**, 49404 (2017).
- [13] M.V. Lunagariya, K.P. Thakor, R.R. Varma, B. Waghela, C. Pathak, M.N. Patel. *Med. Chem. Commun.*, **9**, 282 (2018).
- [14] S. Banerjee, S. Mondal, S. Sen, S. Das, D.L. Hughes, C. Rizzoli, C. Desplanches, C. Mandal, S. Mitra. *Dalton Trans.*, **34**, 6849 (2009).
- [15] W. Kabsch. *Acta Crystallogr. D Biol. Crystallogr.*, **66**, 125 (2010).
- [16] G.M. Sheldrick. *Acta Crystallogr. A.*, **64**, 112 (2008).
- [17] L.J. Farrugia. *J. Appl. Crystallogr.*, **45**, 849 (2012).
- [18] D.J.; Watkin, C.K.; Prout, L.J.; Pearce. CAMERON. Chemical Crystallography Laboratory, Oxford, England 1996
- [19] K. Brandenburg. *DIAMOND*, Bonn, Germany: Crystal Impact GbR, 1999
- [20] S.P. Dash, A.K. Panda, S. Dhaka, S. Pasayat, A. Biswas, M.R. Maurya, P.K. Majhi, A. Crochet, R. Dinda. *Dalton Trans.*, **45**, 18292 (2016).
- [21] N. Biswas, S. Khanra, A. Sarkar, S. Bhattacharjee, D.P. Mandal, A. Chaudhuri, S. Chakraborty, C.R. Choudhury. *New J. Chem.*, **41**, 12996 (2017).
- [22] P. Vijayan, P. Viswanathamurthi, K. Velmurugan, R. Nandhakumar, M.D. Balakumaran, P.T. Kalaichelvan, J.G. Malecki. *RSC Adv.*, **5**, 103321 (2015).
- [23] E. Harder, W. Damm, J. Maple, C. Wu, M. Reboul, J.Y. Xiang, L. Wang, D. Lupyan, M.K. Dahlgren, J.L. Knight, J.W. Kaus, D. Cerutti, G. Krilov, W.L. Jorgensen, R. Abel, R.A. Friesner. *J. Chem. Theory Comput.*, **12**, 281 (2016).
- [24] K. Nakamoto. *Infrared and Raman Spectra of Inorganic and Coordination Compounds*, Wiley, New York 1997 vol. 23.
- [25] A.W. Addison, T.N. Rao, J. Reedijk, J. van Rijn, G.C. Verschoor. *J. Chem. Soc., Dalton Trans.*, **7**, 1349 (1984).
- [26] N. Biswas, S. Saha, S. Khanra, A. Sarkar, D.P. Mandal, S. Bhattacharjee, A. Chaudhuri, S. Chakraborty, C.R. Choudhury. *J. Biomol. Struct. Dyn.*, **37**, 2801 (2019).
- [27] Z. Mandegani, Z. Asadi, M. Asadi, H.R. Karbalaeei-Heidari, B. Rastegari. *Dalton Trans.*, **45**, 6592 (2016).
- [28] M. Muralisankar, S. Sujith, N.S.P. Bhuvanesh, A. Sreekanth. *Polyhedron*, **118**, 103 (2016).
- [29] W.-J. Lian, X.-T. Wang, C.-Z. Xie, H. Tian, X.-Q. Song, H.-T. Pan, X. Qiao, J.-Y. Xu. *Dalton Trans.*, **45**, 9073 (2016).
- [30] A. Rambabu, M.P. Kumar, S. Tejaswi, M.V. Shivaraj. *J. Photochem. Photobiol. B.*, **165**, 147 (2016).
- [31] K.J. Davis, C. Richardson, J.L. Beck, B.M. Knowles, A. Guédin, J.-L. Mergny, A.C. Willis, S.F. Ralph. *Dalton Trans.*, **44**, 3136 (2015).
- [32] N. Muhammad, A. Shah, S. Shuja, S. Ali, R. Qureshi, A. Meetsma, M.N. Tahir. *J. Organomet. Chem.*, **694**, 3431 (2009).
- [33] R.R. Kumar, M.K.M. Subarkhan, R. Ramesh. *RSC Adv.*, **5**, 46760 (2015).

- [34] V.T. Yilmaz, C. Icel, F. Suyunova, M. Aygun, B. Cevatemre, E. Ulukaya. *New J. Chem.*, **41**, 8092 (2017).
- [35] S. Poornima, K. Gunasekaran, M. Kandaswamy. *Dalton Trans.*, **44**, 16361 (2015).
- [36] Z. Shokohi-Pour, H. Chiniforoshan, M.R. Sabzalian, S.-A. Esmaeili, A.A. Momtazi-Borojeni. *J. Biomol. Struct. Dyn.*, **36**, 532 (2018).
- [37] N. Biswas, S. Khanra, A. Sarkar, S. Bhattacharjee, D.P. Mandal, A. Chaudhuri, S. Chakraborty, C.R. Choudhury. *J. Coord. Chem.*, **71**, 2740 (2018).
- [38] P. Anitha, P. Viswanathamurthi, B. Misini, W. Linert. *Monatsh. Chem.*, **144**, 1787 (2013).
- [39] Y.-J. Xiao, Q.-C. Diao, Y.-H. Liang, K. Zeng. *Braz. J. Med. Biol. Res.*, **50**, 6390 (2017).
- [40] P. Sathyadevi, P. Krishnamoorthy, R.R. Butorac, A.H. Cowley, N. Dharmaraj. *Metallomics*, **4**, 498 (2012).
- [41] D. Hegde, S. Dodamani, V. Kumbar, S. Jalalpure, K.B. Gudasi. *Appl. Organomet. Chem.*, **31**, 3851 (2017).
- [42] M.A. Malik, O.A. Dar, P. Gull, M.Y. Wani, A.A. Hashmi. *Medchemcomm.*, **9**, 409 (2018).
- [43] R. Manikandan, P. Viswanathamurthi, K. Velmurugan, R. Nandhakumar, T. Hashimoto, A. Endo. *J. Photochem. Photobiol. B.*, **130**, 205 (2014).
- [44] M. Pellei, L. Bagnarelli, L. Luciani, F.D. Bello, G. Giorgioni, A. Piergentili, W. Quaglia, M.D. Franco, V. Gandin, C. Marzano, C. Santini. *IJMS*, **21**, 2616 (2020).
- [45] S. Selvamurugan, R. Ramachandran, P. Viswanathamurthi. *Biometals*, **26**, 741 (2013).
- [46] B.-L. Fei, Z.-X. Huang, W.-S. Xu, D.-D. Li, Y. Lu, W.-L. Gao, Y. Zhao, Y. Zhang, Q.-B. Liu. *J. Photochem. Photobiol. B.*, **160**, 43 (2016).
- [47] A.V. Eremin, R.V. Suezov, P.S. Grishina, A.I. Ponyaev, N.L. Medvedskiy. *Mediterr. J. Chem.*, **7**, 28(2018).